Sensitivity and Optimization of Localized Surface Plasmon Resonance Transducers

Ofer Kedem, Alexander B. Tesler, Alexander Vaskevich,* and Israel Rubinstein*

Department of Materials and Interfaces, Weizmann Institute of Science, Rehovot 76100, Israel

ABSTRACT Gold nanoisland films displaying localized surface plasmon resonance optical response were constructed by evaporation on glass and annealing. The surface plasmon distance sensitivity and refractive index sensitivity (RIS) for island films of different nominal thicknesses and morphologies were investigated using layer-by-layer polyelectrolyte multilayer assembly. Since the polymer forms a conformal coating on the Au islands and the glass substrate between islands, the relative sensitivity of the optical response to adsorption on and between islands was evaluated. The RIS was also determined independently using a series of solvents. An apparent discrepancy between the behavior of the RIS for wavelength shift and intensity change is resolved by considering the different physical nature of the two quantities, leading to the use of a new variable, that is, RIS (for intensity change) normalized to the surface density of islands. In the present system the surface plasmon decay length and RIS are shown to be directly correlated; both parameters increase with increasing average island size. This result implies that a higher RIS is not always beneficial for sensing; maximizing the transducer optical response requires the interrelated RIS and decay length to be optimized with respect to the dimensions of the studied analyte-receptor system. It is shown that, as a rule, transducers comprising larger islands furnish better overall sensitivity for thicker adlayers, whereas thinner adlayers produce a larger response when sensed using transducers comprising smaller islands, despite the lower RIS of the latter.

KEYWORDS: localized plasmon · LSPR · sensitivity · gold · islands · decay length · optimization

Nanosized metal (*e.g.*, gold, silver) structures exhibit an extinction band in, or close to, the visible range, which is not present in the bulk metal spectrum. This band is attributed to localized surface plasmon resonance (LSPR), that is, excitation of localized surface plasmons (also known as plasma polaritons).[1] The characteristics of this resonance are affected by the size, shape, and substance of the nanostructures, as well as by plasmon coupling effects in the case of ensembles.[2−4] The wavelength, intensity, and shape of the LSPR band are sensitive to changes in the dielectric properties of the surrounding, including changes induced by binding of molecules to the metal structures, displacing air or solvent.[5] The latter forms the basis for application of LSPR systems as optical transducers for chemical and biological sensing.[6] Our group has concentrated on LSPR systems based on random-type Au island films prepared by vacuum evaporation and postdeposition annealing.[7]

The magnitude of the LSPR transducer response depends on factors mentioned above, as well as on the distance from the metal surface. This dependence stems from the decay of the evanescent plasmon field, extending from the metal structure into the surrounding medium. This decay, which depends on the type of metal and physical parameters of the nanostructures, was found to be described reasonably well by[2,8]

$$R = m\Delta\eta[1 - \exp(-d/l)] \qquad (1)$$

where R is the transducer response (wavelength shift or intensity change); m is the refractive index sensitivity (RIS), that is, peak shift or intensity change per refractive index unit (RIU) change; $\Delta\eta$ is the change in refractive index (RI) of the surrounding medium effected by the adsorbate; d is the dielectric (adsorbate) layer thickness; and l is the plasmon effective decay length.[9,10] Note that eq 1 is commonly written with a factor of 2 in the exponent numerator;[9,11] we chose here to eliminate this factor as the relationship expressed in eq 1 is rather empirical. We therefore refer to l as the effective decay length. The physical model presented by eq 1 relates to the measurement of extinction and does not distinguish between absorption and scattering; however, it can serve as a good approximation in sensing applications. A more elaborate treatment should include independent reflection and transmission measurements[12] and is currently in progress.

As noted above, the sensitivity of LSPR transducers to the dielectric properties of the local environment can be exploited for sensing purposes. Typically, a recognition layer is first immobilized on the metal nanostructures, for example, an antibody, and a UV/vis/NIR (depending on the specific transducer) spectrum is recorded, showing

*Address correspondence to alexander.vaskevich@weizmann.ac.il, israel.rubinstein@weizmann.ac.il.

Received for review May 13, 2010 and accepted December 29, 2010.

Published online January 12, 2011
10.1021/nn102617d

the LSPR band. The transducer is then exposed to the unknown solution; if the latter contains the specific analyte (*e.g.*, an antigen specific to the immobilized antibody), it will bind to the recognition layer, and a change in the spectrum will be detected.[6,9] The response in such a scenario is described by eq 2:

$$R = m\Delta\eta \exp(-d_1/l)[1-\exp(-d_2/l)] \qquad (2)$$

where d_1 and d_2 are the thicknesses of the recognition interface and the analyte layer, respectively. According to eq 2, to obtain maximal response to analyte binding one has to maximize the RIS m and match the decay length l to the analyte and recognition interface dimensions.

While the quest for maximal RIS is straightforward, the issue of the decay length is more complex. Binding of the analyte takes place at a certain distance from the metal surface, determined by the dimensions of the recognition layer and the analyte. If the decay length is small with respect to the dielectric layer thickness, the rapid exponential decay will lead to a weak response to the binding event. If, on the other hand, the decay length is large compared to the dielectric layer thickness, the analyte will occupy a small fraction of the sensing volume, leading, again, to a weak response. Thus, for optimal response a transducer has to be chosen such that the combined RIS and decay length maximize the response to a given analyte−receptor system.[13,14]

The decay length in LSPR systems has been previously investigated. Van Duyne and co-workers examined triangular Ag nanoisland films fabricated by nanosphere lithography;[15] the response to adsorption of dielectric layers, seen as a red-shift of the extinction peak, was found to be linear with distance in the short-range (several nm),[16] and exponentially decaying in the medium range (tens of nm).[17] It was found that for equal in-plane dimensions, the decay length is larger for particles with smaller out-of-plane height.[18] Work on surface-immobilized Au colloids found a positive relationship between particle size and decay length.[13,19] Our group has studied the distance dependence of LSPR extinction in a system comprising coordination-based multilayers of varying thickness adsorbed onto evaporated Au island films.[20] In another work a semi-quantitative relationship was shown between distance and LSPR response in biological sensing.[11] Interestingly, it was found that in the long-range (hundreds of nm) the response to adsorption of additional layers oscillates between a red shift and a blue shift.[21−23]

The phenomenological model presented by eq 1 assumes that both parameters defining the optical response (RIS and decay length) are spatially invariant, while calculations[24] and recent experiments[25] show spatial variations. In the case of island size and shape distribution (as in the present system), the model also does not take into account variations in sensitivity between different islands in the film. In practice we measure a macroscopic area of the island film, thereby averaging over islands and binding sites with possibly different sensitivities and decay lengths. Our earlier work presented evidence for effective averaging in our system, manifested as a linear optical response to binding of small (<2 nm) adsorbates on Au island films, for fractional coverages from *ca.* 0.01 to a full monolayer.[26,27]

A common technique for obtaining thin films of well-defined thicknesses in the nanometer range is layer-by-layer (LbL) deposition, in which a layered nanostructure is built up in a stepwise fashion. In the present work we have used the polyelectrolyte LbL approach introduced by Decher and co-workers, involving alternate binding of oppositely charged polyelectrolyte layers *via* electrostatic interactions.[28] This widely used approach is noted for its simplicity and repeatability.[29,30] The thickness of the repeated layers depends strongly on the ionic strength of the deposition solution, with higher ionic strengths resulting in thicker layers.[31,32]

The LbL polyelectrolyte deposition scheme is used here for obtaining dielectric coatings of systematically varying thicknesses, with the aim of determining the decay length and RIS of island-type Au films of different morphologies. The advantages of polyelectrolyte multilayers are simplicity, reproducibility, and a highly controlled thickness. A noted complication is the fact that the resulting layer forms a conformal coating on the islands and on the glass substrate between the islands, thus deviating from the simple exponential model which assumes homogeneous growth on the entire island surface. To justify the use of eq 1 we therefore had to evaluate the relative sensitivity of the transducer to buildup of a dielectric layer on the islands *versus* between islands.

We set out to obtain systematic data on the sensing parameters (decay length and RIS) of a series of Au island films and study possible relationships between these parameters and physical variables of the islands (*e.g.*, average island dimensions), as well as a possible correlation between the two parameters. Such relationships can be used for rational design and optimization of LSPR transducers for sensing of specific analytes.

RESULTS AND DISCUSSION

Transducer Preparation. Gold island films of 3, 4, 5, 6, 7.5, 9, and 10 nm (nominal thickness) were fabricated by evaporation on glass followed by annealing 10 h at 580 °C, as detailed in the Methods section. We have previously shown that the high-temperature annealing promotes partial embedding and stabilization of the Au islands on the glass,[33] while lowering somewhat the RIS due to reduction of the exposed Au area.[7] Figure 1 panels A−C show representative high-resolution scanning electron microscopy (HRSEM) images of samples of 3, 5, and 10 nm (Au nominal thickness), covered with

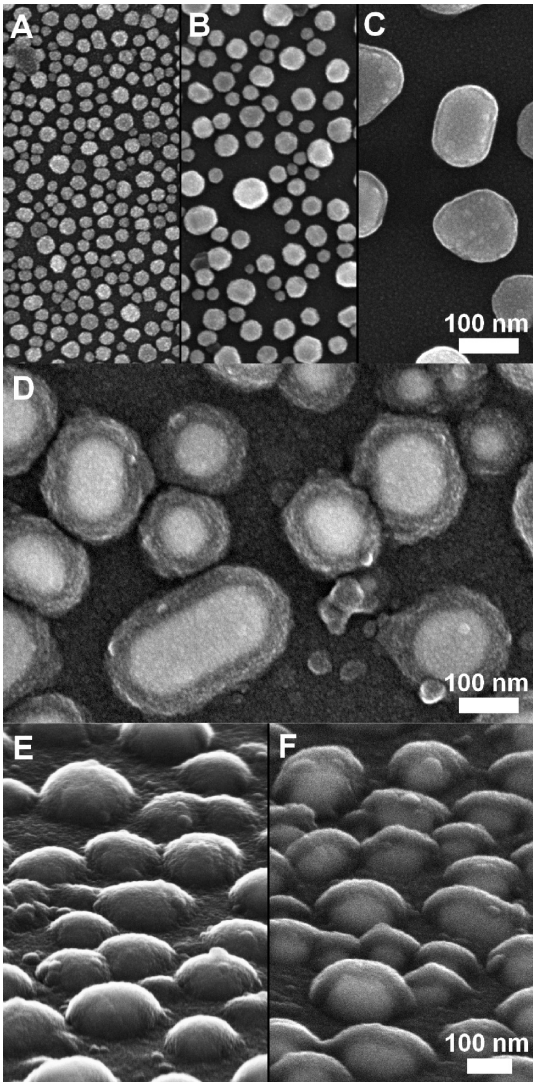

Figure 1. HRSEM images of gold island films of (A−C) 3, 5, and 10 nm (nominal thickness), annealed. Slides A, B, and C were coated with 2, 2, and 3 nm Cr, respectively, prior to imaging; (D−F) 10 nm (nominal thickness) Au islands coated with 40 polyelectrolyte layers, in plan view (D) and in isometric view (60° from normal), showing the surface (E) and internal composition (F); samples were coated with 3 nm Cr prior to imaging. Accelerating voltages were 15 kV (A−D) and 20 kV (E, F); in-lens (A−E) and chamber-mounted Everhart−Thornley (F) secondary-electron detectors were used.

a thin Cr layer to improve the conductivity. The images were analyzed as described in the Methods section.

Table 1 presents average values of the Au island major and minor axes, the fraction of the image area covered by Au particles, the effective height (calculated as the nominal thickness divided by the coverage, representing material distribution rather than average island height), the particle aspect ratios, the mean interparticle distance (center-to-center), and the particle surface density. Note that the Cr coating may have a marginal effect on the analysis results.

With increase of the film nominal thickness, which is the only independent parameter, the average island dimensions gradually increase, while the coverage tends to become smaller and the average interisland distance becomes larger (Table 1), as a result of gold accumulating into larger islands with a higher volume-to-surface ratio. While the out-of-plane aspect ratio remains rather unchanged, the in-plane aspect ratio shows a tendency to increase at higher nominal thicknesses. The correlations between the various parameters make the evaluation of the impact of individual parameters on the transducer sensitivity (see below) quite difficult.

Island dimensions and interparticle distances show a sharp increase between 6 and 7.5 nm, separating two populations of islands which can be classified according to the morphology of the as-evaporated (unannealed) films: small (isolated, 3 to 6 nm) and large (near-percolated and percolated, 7.5 to 10 nm).[7] The island surface density was calculated from analysis of SEM images.

Figure 2 shows characteristic extinction spectra of Au island films (bare Au, annealed; see Methods). The wavelength of the surface plasmon band is affected by various factors, including interisland distance, island size distribution, aspect ratio, and embedding depth in the glass substrate. The ratio of (average) interisland distance to (average) island major axis increases from 1.2−1.3 for 3−6 nm island films to 1.4−1.5 for thicker films, implying a decrease of the surface plasmon coupling. The latter is expected to result in a blue shift of the surface plasmon band. However, other factors, such as increase of the average island size and aspect ratio, become dominant with increasing nominal thickness, resulting in a near constant wavelength of the surface plasmon band for the small islands and a red-shift of the band for the larger islands (Figure 2). Numerical modeling using the discrete dipole approximation (DDA) method and taking into account the experimental island size distributions, showed a semi-quantitative agreement between the calculated and measured spectra for the larger islands; that is, the surface plasmon peak shifted to the red and the intensity increased with the nominal thicknesses.[34]

Polyelectrolyte Multilayers. For polyelectrolyte LbL assembly, slides to be coated were alternatingly immersed in PAH and PSS solutions, as detailed in the Methods section. The first layer of PAH was adsorbed directly on the Au surface, exploiting the interaction of amine groups with Au. A prerequisite for the use of polyelectrolyte LbL assembly for construction of dielectric layers of well-defined thicknesses is that every deposition cycle (PAH/PSS bilayer) adds the same amount of material and the same thickness, for a large number of layers. The PAH/PSS system used in the present work is known to grow in a linear fashion.[35] To test this behavior in our hands, polyelectrolyte multilayers were constructed on glass and quartz slides coated with a 20-nm-thick semitransparent continuous Au film. The regularity of the growth can be followed by monitoring the PSS absorption peaks at 194 and

TABLE 1. Statistical Data for Morphology of Annealed Gold Island Films

nominal thickness (nm)	coverage (%)	effective height (nm)	average axis (nm) major	average axis (nm) minor	aspect ratio in-plane[a]	aspect ratio out-of-plane[b]	average interparticle distance (nm)	particle surface density (cm^{-2})
3	49.8	6	22.3 ± 4.9	20.1 ± 4.5	1.11 ± 0.08	3.5 ± 0.8	27.3 ± 4.2	1.6×10^{11}
4	50.2	8	27.1 ± 6.6	23.8 ± 5.9	1.14 ± 0.10	3.2 ± 0.8	32.6 ± 4.8	9.3×10^{10}
5	40.9	12.2	34.2 ± 9.6	31.1 ± 8.7	1.10 ± 0.07	2.7 ± 0.8	46.1 ± 8.9	4.4×10^{10}
6	52.0	11.5	39.9 ± 10.6	35.7 ± 10.3	1.14 ± 0.11	3.3 ± 0.9	48.3 ± 7.7	4.2×10^{10}
7.5	36.5	20.5	73.5 ± 22.2	64.3 ± 18.2	1.14 ± 0.10	3.4 ± 1.0	105.4 ± 18.8	9.2×10^{9}
9	35.1	25.6	79.0 ± 30.4	66.9 ± 23.2	1.17 ± 0.14	2.8 ± 1.0	111.7 ± 22.1	7.3×10^{9}
10	31.3	31.9	113.5 ± 41.1	92.4 ± 28.3	1.22 ± 0.17	3.2 ± 1.1	168.7 ± 27.8	2.8×10^{9}

[a] Major axis divided by the minor axis. [b] Average of major and minor axes divided by the effective height.

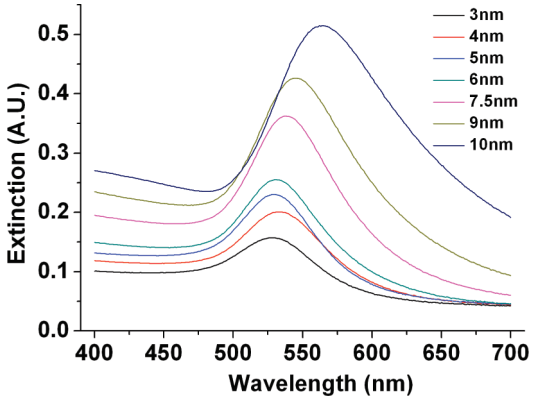

Figure 2. Representative extinction spectra of gold islands films for various nominal thicknesses (indicated). Extinction is given in absorbance units (A.U.).

227 nm.[28,36] Au films on quartz slides were measured (in air) by transmission UV/vis spectrophotometry during the LbL process. A linear relationship between the number of cycles and the UV peak intensity was found (Figure S1, Supporting Information), indicating regular growth of the deposited mass. A small decrease in the extinction in the visible range with added layers was also observed, attributed to the antireflective nature of the coating in this spectral range.

Quartz and glass slides were dried and measured by spectroscopic ellipsometry after adsorption of different numbers of polyelectrolyte layers. The thickness of the multilayers was determined and plotted as a function of the number of layers. Figure S2 (Supporting Information) shows the data points and a linear regression line (R^2 = 0.99531), indicating that each PAH/PSS bilayer is 2.09 ± 0.03 nm thick. The ellipsometric analysis also provided a value of *ca.* 1.56 for the refractive index (RI) of the polyelectrolyte multilayer in the visible range. These values were used throughout the work, assuming that the thickness of the polyelectrolyte layers on Au islands is the same as that on continuous Au substrates. It was also found that drying the slides between deposition steps did not affect the final thickness or the adsorbed mass.

Site-Selective Adsorption. LSPR measurements of LbL polyelectrolyte multilayer formation in the present system involves three kinds of averaging, deriving from the macroscopic nature of the measurements: (i) adsorption at different locations on the Au island surface, possibly having differing sensitivities;[24,25] (ii) adsorption on islands of different shapes and sizes; (iii) adsorption on the islands and on the glass substrate between the islands. Regarding the first two points, we have previously established the validity of averaging over the different sizes, shapes and surface binding sites of the islands in the ensemble.[26,27]

To examine the effect of binding on islands *versus* binding between islands, dielectric monomolecular layers were selectively adsorbed on the Au islands or on the glass between the islands, using 1-octadecanethiol (ODT) and a trimethoxysilane-terminated polyethyleneglycol (PEG-silane), respectively. The thickness of ODT and PEG-silane self-assembled monolayers (SAMs) is known to be approximately 2 nm,[37,38] and their refractive indices are close to 1.5. For each Au nominal thickness, samples were coated either with ODT followed by PEG-silane, or in the reverse order. The procedure is illustrated in Figure 3; note the subtle difference in the final structures in the vicinity of the Au/glass/adlayer interface.

Figure 4 panels A and B show representative spectra of 4 nm (nominal thickness) Au island films before and after coating with SAMs according to the two schemes in Figure 3. In both cases adsorption of ODT (on islands) promotes a considerably larger response compared to assembly of PEG-silane (between islands). The results for a range of Au island sizes (Figure 4C) indicate the following: (i) The difference in the response (as wavelength shift) to ODT and PEG-silane applies to all measured sizes. (ii) The response to a given molecule is always larger when it is adsorbed first; this is consistent with the illustration in Figure 3, showing the different occupancy of the Au−glass−air interface region for the different assembly sequences. (iii) The response generally decreases with increasing island size, reflecting the effect of the growing decay length,

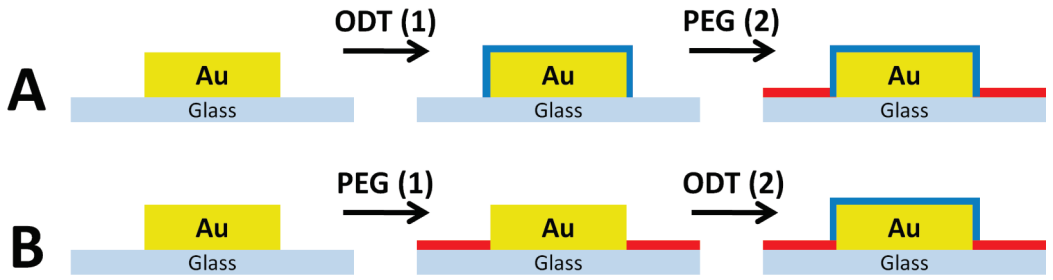

Figure 3. Illustration of the two schemes of site-selective monolayer assembly. Dimensions are not to scale.

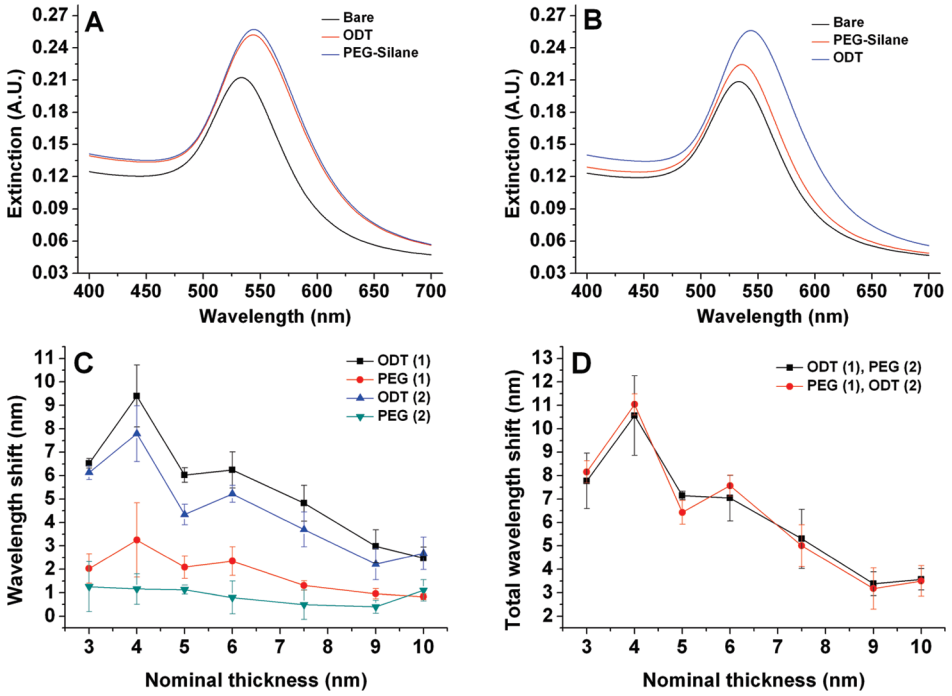

Figure 4. Transmission UV−vis spectra of 4 nm Au island films: (A) adsorption of ODT followed by PEG-silane; (B) adsorption of PEG-silane followed by ODT; (C) peak wavelength shift for adsorption of each layer; (D) overall wavelength shift for the two types of samples. The lines in panels C and D are guides to the eye. Data points are the average of four slides each; error bars are standard deviation.

as further discussed in the next section. (iv) For a full monolayer coating of the samples, the response is attributed primarily to the SAM fraction adsorbed on the Au islands, while the contribution of the fraction adsorbed on the glass is considerably smaller.

The significance of the results in Figure 4D, showing that the combined response of the two assembly steps is the same in both cases, is in verifying that the system is well-behaved and the assumption of site-selective self-assembly is valid. The results of the site-selective adsorption experiments substantiate the use of polyelectrolyte multilayers for determination of decay length in our system, as elaborated below.

Effective Decay Length. To determine the effective decay length and RIS of Au island films of different nominal thicknesses, polyelectrolyte multilayers were deposited on the Au islands in a manner similar to that described above for continuous Au substrates, and transmission spectra were measured after the binding of each bilayer. Four slides were measured for each Au island thickness. The LbL assembly was carried out until the characteristic parameters (plasmon peak wavelength and intensity) showed a tendency to stabilize.

Figure 1D presents a HRSEM plan-view image of a gold island slide coated with a polyelectrolyte multilayer, showing a rather uniform polymer layer around the islands. An isometric view (60° from normal) of the same sample is presented in Figure 1 panels E and F, utilizing different detectors to show, respectively, the surface and the internal composition. The thickness of the 40-layer film, determined from Figure 1D, is 40 ± 4 nm, in agreement with the thickness measured by ellipsometry on continuous gold (Figure S2, Supporting Information).

The images in Figure 1 panels E and F indicate that the polyelectrolyte multilayer forms a conformal coating on the gold islands and the glass surface between the islands.[39] This morphology presents a complication in the use of eq 1, the latter assuming a homogeneous dielectric film around the islands. However, on the basis

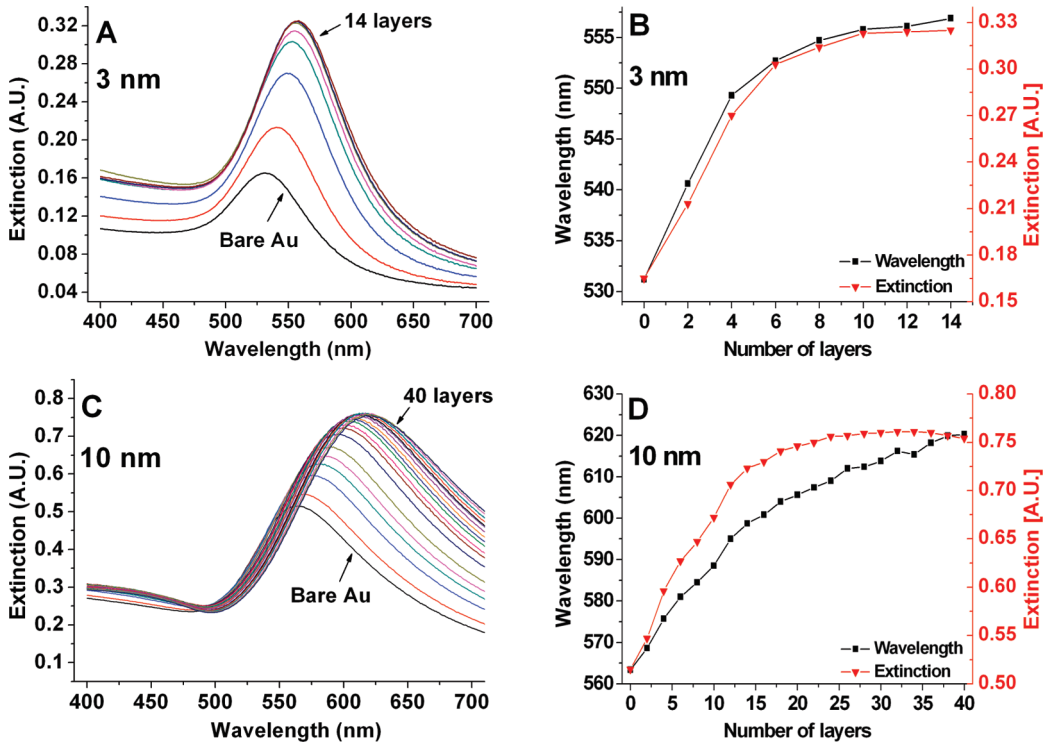

Figure 5. Representative spectra (A, C) and plasmon peak wavelength and extinction intensity (B, D; experimental points are connected for viewing convenience) for increasing number of polyelectrolyte layers on Au islands of indicated nominal thicknesses. Spectra recorded after assembly of each bilayer.

of the results in the previous section, showing that the major part of the response to a conformal monomolecular coating is attributed to the fraction on the metal islands, it can be shown that the optical behavior of the Au island transducer/polyelectrolyte multilayer system is reasonably well described by eq 1 (see Discussion section and Supporting Information).

Figure 5 shows representative spectra and plasmon peak wavelength and intensity for polyelectrolyte LbL assembly on 3 and 10 nm Au island films, exhibiting the increase in the decay length with nominal thickness. In sensing applications the optical response is usually quantified as the surface plasmon wavelength shift or intensity difference, the latter measured either at the surface plasmon band maximum[40] or at a constant wavelength close to the maximal intensity change.[20,40] Figure 6 shows the plasmon wavelength shift and extinction intensity change, both at the extinction peaks and at a constant wavelength (570 nm), for coating of a 3 nm Au island film with polyelectrolyte multilayers of increasing thickness. The plots include exponential fits to eq 1. Given the experimentally measured R (the response, as wavelength shift, R_λ, or extinction intensity change, R_{ext}) and d (polyelectrolyte multilayer thickness), the regression provides the effective decay length l for wavelength (l_λ) or intensity (l_{ext}), as well as the product $m\Delta\eta$ of the RIS, m (as m_λ or m_{ext}) and the difference in RI, $\Delta\eta$, between the medium (in the present case, air) and the dielectric layer. The ellipsometrically determined value of 1.56 for the RI of the

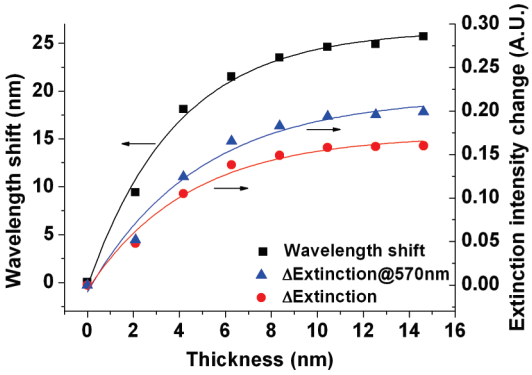

Figure 6. Exponential fits of the plasmon wavelength shift (black squares) and intensity change at the peak (red circles) and at a constant wavelength of 570 nm (blue triangles), as a function of polyelectrolyte multilayer thickness, for 3 nm (nominal thickness) Au island films. Data extracted from Figure 5 panels A and B.

dielectric layer (see above) gives $\Delta\eta = 0.56$, hence the RIS m_λ or m_{ext} can be derived from the same data.

Exponential regression of the data in Figure 6 provides the values 3.9 ± 0.3 nm and 47.9 ± 1.6 nm/RIU for l_λ and m_λ, respectively; 4.4 ± 0.7 nm and 0.316 ± 0.018 A.U./RIU for l_{ext} and m_{ext} measured at the peak; and 4.8 ± 0.8 nm and 0.400 ± 0.027 A.U./RIU for l_{ext} and m_{ext} measured at 570 nm. The decay length values calculated at the surface plasmon maximum or at a single wavelength are therefore consistent within the experimental uncertainty. Note that in what follows we use RIS values (m_{ext}) measured at the peak.

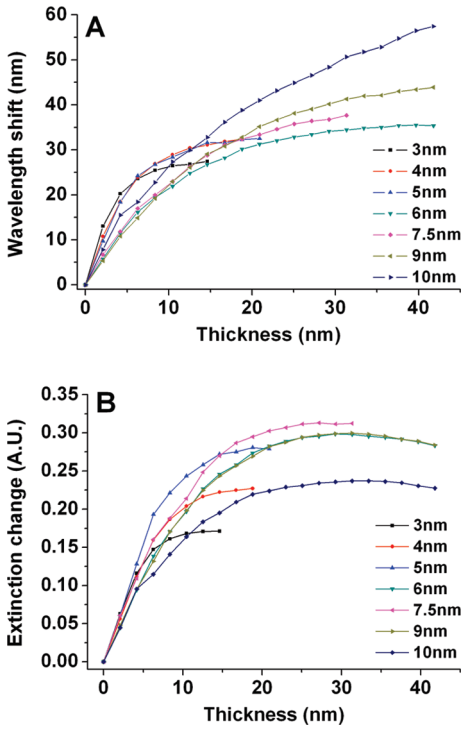

Figure 7. Plasmon peak wavelength shifts and extinction intensity change for the deposition of polyelectrolyte layers on Au island films of indicated nominal thicknesses; values are an average of four slides per Au thickness. Experimental points are connected for viewing convenience.

A compilation of data on plasmon peak wavelength and intensity for all the Au thicknesses studied is shown in Figure 7, presented as difference values. Generally, with increased Au thickness (*i.e.*, larger islands), thicker polyelectrolyte coatings are needed to approach saturation (Figure 7),[20] indicating a larger decay length. Note that for films of 6 nm and above, the peak wavelength and intensity reach a maximum and start to decrease after a certain number of layers, with the wavelength lagging behind (Figure 5D and Figure 7, wavelength decrease not seen yet). This phenomenon is related to long-range LSPR effects,[21,23] seen in our system for assembly of thick polyelectrolyte layers on large Au islands.[41] Another effect which may influence the shape of the curves in Figure 7 is filling of the gaps between islands as more layers are added. These effects, which are not described by eq 1, become important for thick coatings.

To minimize the effect of these deviations, in the curve fitting only data points up to the maximum extinction (Figure 6) were used for the exponential fit of the intensity change. This treatment is justified as our approach in the present work is largely empirical and assumes that eq 1 provides a reasonable description of the system's optical response. Therefore, the values of the decay length *l* and the RIS *m* extracted from the exponential regression are to be considered effective parameters, which are important in evaluating sensing capabilities. Understanding the physical

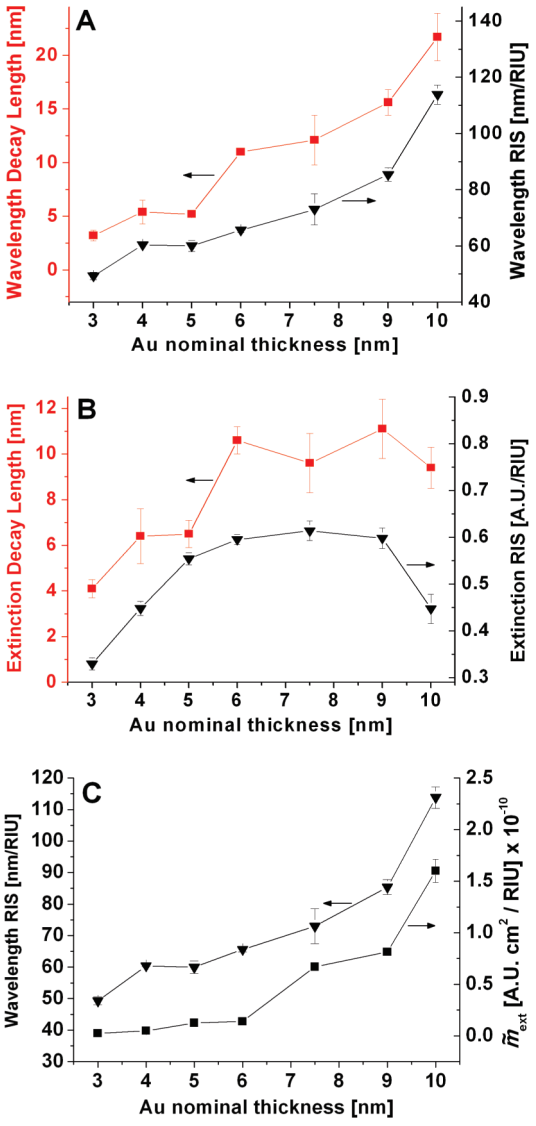

Figure 8. (A) Wavelength and (B) extinction intensity decay length and refractive index sensitivity (RIS) from exponential regression, *vs* Au nominal thickness. (C) Wavelength RIS and normalized intensity RIS *vs* Au nominal thickness. Error bars represent standard deviation or average standard error (larger of the two) of four samples per Au thickness.

basis requires a more elaborate approach which is beyond the scope of the present work.

Average decay length and RIS values, determined using the exponential fit, are summarized in Figure 8 panels A and B. The wavelength decay length and RIS values exhibit a regular increase with increasing nominal thickness and average island size (Figure 8A). The intensity decay length values increase with a tendency to saturate, while the values of the intensity RIS show an initial increase and a decrease for larger islands (Figure 8B). The difference in the values of the wavelength and intensity decay length for larger islands (Figure 8 panels A and B) is likely to be related to long-range localized plasmon interactions, as noted above. The different behavior of the RIS for wavelength (monotonous increase, Figure 8A) and intensity (maximum around 7.5 nm, Figure 8B) is attributed

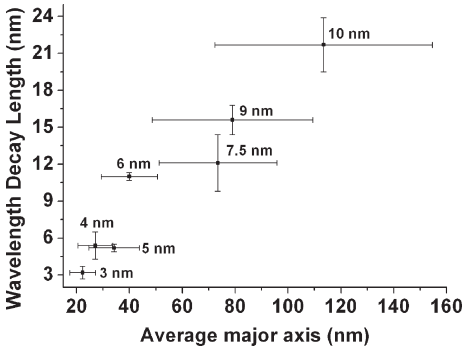

Figure 9. Decay length (for wavelength shift) *vs* average major axis of Au islands, for samples of varying Au nominal thicknesses (indicated). Error bars represent standard deviation.

primarily to the fundamental difference between the two physical parameters, as further elaborated in the Discussion section.

The results shown in Figure 8 are highly significant, presenting a general correlation between the decay length and RIS, for both wavelength and extinction intensity. This point is further elaborated in the Discussion section. Using the statistical analysis of HRSEM images described above, the relationship between Au island size and decay length is presented in Figure 9 as the wavelength decay length *versus* the average Au island major axis. Although the experimental error bars are quite large and increase with island size, the figure shows a clear correlation between the two parameters.

Refractive Index Sensitivity. The RIS of samples of various Au thicknesses was determined independently by measuring extinction spectra in a series of solvents of varying RI values, which is the common method of determining the RIS of optical transducers. The RI of the different solvents was measured using an Abbe refractometer. The solvents used were (RI in parentheses) methanol (1.328), ethanol (1.359), heptane (1.386), chloroform (1.445), and toluene (1.496). Since the solvent layer thickness is practically infinite relative to the decay length, eq 1 is reduced to $R = m\Delta\eta$, and the RIS m can be extracted from the slope of R *vs* $\Delta\eta$, using linear regression and assuming that m is independent of the RI in the measured range.

Figure 10 shows representative results for a 4 nm Au island film, illustrating the procedure used for obtaining the RIS values: (a) spectra are measured in the various solvents; (b) the peak wavelength and intensity are plotted *versus* the medium RI, and the RIS values m_λ and m_{ext} are determined using a linear fit. Four samples were used for each thickness. While the optical parameters change quite linearly in the different solvents as expected from the linear approximation of eq 1, the experimental points in air ($\eta = 1.00$) deviate from linearity and their inclusion in the calculation requires a higher order treatment. For simplicity, the results in air were not included in the determination of the RIS. From the linear regressions (Figure 10B) it was determined that

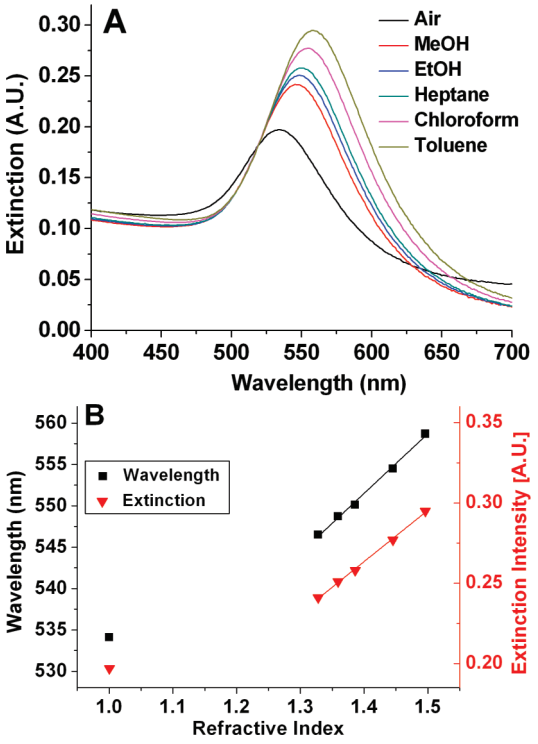

Figure 10. Representative results for a 4 nm (nominal thickness) Au island film: (A) spectra in air and in various solvents; (B) plasmon peak wavelength and intensity *vs* refractive index of the medium, and linear regressions to the data in solvents. Error bars in panel B are too small to be seen.

the RIS (wavelength) is 72.2 ± 2.5 nm/RIU, and the RIS (extinction intensity) is 0.319 ± 0.008 A.U./RIU.

Figure 11 presents the RIS m_λ *versus* the wavelength of the bare Au plasmon peak, for the different thicknesses. The data suggest a correlation with a minimum at plasmon band wavelengths of *ca.* 537 nm. A positive correlation between the surface plasmon wavelength and the RIS, with rather large data scatter, was previously shown.[7,42] A discussion of our current results should take into account various parameters, such as the distribution of island size, shape, and interisland distance, and is outside the scope of the present work.

A comparison of RIS values obtained using the two methods, that is, exponential fit of multilayer results *versus* direct measurement in different solvents, is presented in Figure 12. For all the nominal thicknesses studied, the RIS values measured using the two methods exhibit the same qualitative behavior. However, m_λ values measured directly are larger by *ca.* 10−30% than those determined by the exponential fit, whereas m_{ext} values measured directly are smaller by *ca.* 20−40%.

Factors that may be responsible for the differences between the RIS values determined by the two methods include the following: (i) The multilayer thickness and RI extracted from ellipsometry on continuous Au and used for the exponential fit may be somewhat different from the values on Au islands. (ii) The exponential fit includes the difference in RI $\Delta\eta$ between the

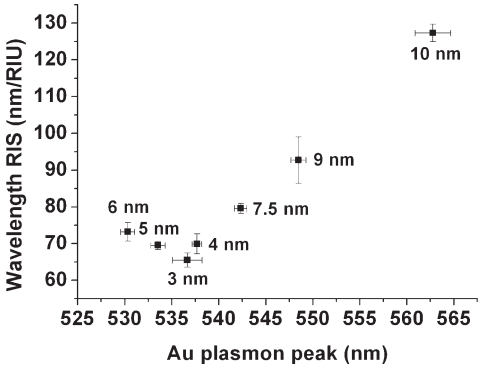

Figure 11. Refractive index sensitivity m_λ *vs* wavelength of the plasmon peak for Au island films of various nominal thicknesses (indicated). Error bars represent the standard deviation of four samples for each Au thickness.

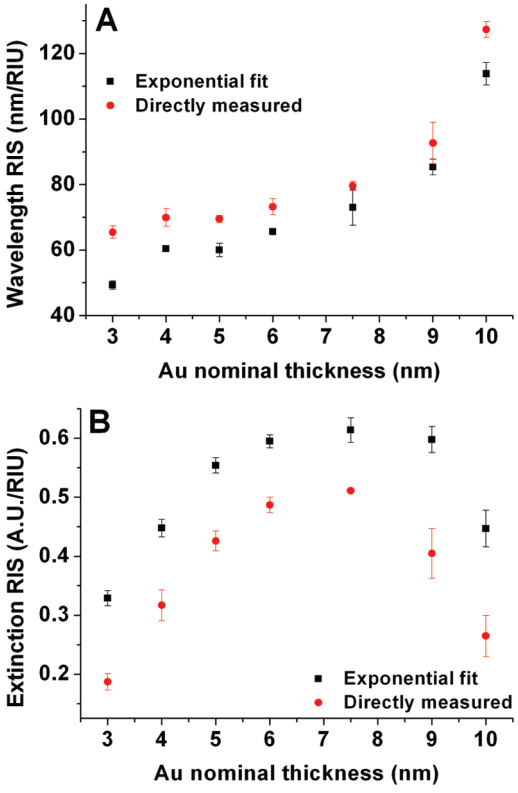

Figure 12. Refractive index sensitivity (RIS) values obtained by exponential regression of LbL results and values measured directly using a series of solvents, for wavelength shift (A), and extinction intensity change (B).

multilayer (1.56, from ellipsometry) and air (1.00), assuming a linear response in this range. However, as discussed above (Figure 10), the experimental data show a linear behavior in the range used for direct RIS measurement (1.328−1.496) but not in the range used for the exponential treatment. (iii) The assumption of a regularly increasing film thickness fails when the growing films on adjacent islands begin to overlap. (iv) Equation 1 assumes that the response is monotonous with increasing film thickness, from zero to infinite thickness (the equivalent of changing the solvent); however, as noted in the introduction, at increased dielectric layer thicknesses the response was found to oscillate.[21−23,41] Hence, the simple exponential model used for the polyelectrolyte multilayers may not extend monotonously to the bulk. Given all these factors, the general agreement between the RIS values determined by the two methods is satisfactory.

Discussion. We chose to study the characteristic optical properties of LSPR transducers using polyelectrolyte LbL multilayers, as such coatings are easy to prepare, reproducible, and the thickness is well controlled. However, the growth mode of these films introduces a deviation from the model described by eq 1, namely, coating of the glass between the islands and gradual filling of the free space between islands as the multilayer thickness grows. It was therefore essential to show that these deviations have a minor effect on the optical response, thus justifying data analysis using the simple exponential model.

The site-selective adsorption experiments indicated that the response to SAM deposition between the islands is much weaker than the response to similar deposition on the islands. Using these results as well as the known average dimensions of the islands, the dielectric film characteristics, and the measured response to polyelectrolyte binding, the relative contribution of coating of the glass between the islands to the overall response was derived (see Supporting Information for details). The calculation shows that the fraction of the overall response generated by deposition on the glass decreases as the layer thicknesses increases, due to the exponential decay of the plasmon field. Hence, for a 5 nm Au island film, the part of the response attributed to deposition on the glass decreases from *ca.* 19% to *ca.* 6% as the layer thickness grows from 1 to 12 nm.

It is therefore concluded that despite the complex process, a simple exponential model describes the optical behavior of the present system in a satisfactory manner, even under conditions where the gap between islands is largely filled by the recognition interface and bound analyte.

The decay length of LSPR transducers has been previously investigated in a wide variety of systems, including nanosphere lithography (NSL) fabricated triangular Ag and Au arrays,[18,22,24] chemically synthesized Ag and Au nanoparticles,[3] both in solution[43] and adsorbed on surfaces,[19,40,44] and thermally evaporated Au particles on substrates.[20,21,45] Exponential decay of the plasmon field was commonly assumed, and in general larger particles exhibited a longer decay length. Most studies included particles of a single size, and only a few presented actual decay length values.

The need to consider both the RIS and decay length for LSPR transducer optimization is inherent in eqs 1 and 2, and was recognized previously.[13,14] This issue was also addressed in the context of comparing the sensitivity of LSPR to that of propagating surface plasmon resonance (SPR),[1,12] where the smaller decay

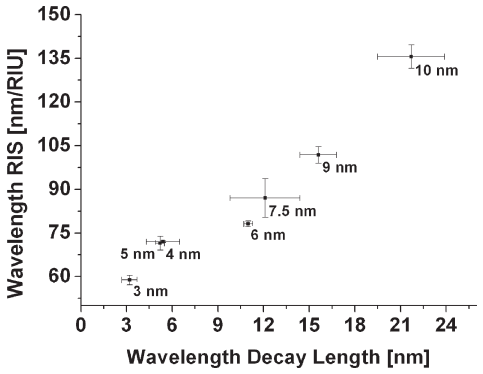

Figure 13. Refractive index sensitivity for wavelength shift as a function of wavelength decay length (both from exponential regression of LbL results), for the various Au nominal thicknesses studied (indicated).

length of LSPR transducers is said to compensate for their lower RIS. However, the existence of a direct correlation between the decay length and RIS in localized plasmon systems has not been demonstrated.

As shown in Figure 8A, films with larger islands feature both higher RIS and decay length values. Hence, the two parameters are strongly linked; the experimental correlation is presented in Figure 13. The implications of this correlation are far-reaching in terms of sensing. Common analytes and recognition interfaces (notably, biological molecules) are several nm in size, meaning that choosing transducers with high RIS values inevitably leads to poor matching of the decay length (Figure 13). To maximize the response it is therefore imperative to find the optimal combination of RIS and decay length, which has to be tuned to the specific analyte and recognition layer dimensions.

To demonstrate optimization of the transducer response, Figure 14 shows the incremental change in plasmon peak wavelength and intensity resulting from adsorption of a 2.1-nm-thick polyelectrolyte bilayer (PAH/PSS) on an existing polyelectrolyte multilayer of varying thickness. This exercise simulates binding of a 2.1 nm analyte on a dielectric recognition layer of varying thickness. The figure features graphs calculated by substituting the experimental decay length and RIS values (Figure 8) in eq 2. The simple exponential model is satisfactory in providing a semiquantitative description of the response of these systems, with the wavelength shift showing better reproduction of the experimental data (compare Figure 14 to Figure S3, Supporting Information).

As seen in Figure 14 (most clearly in Figure 14A), the optical response to binding of a 2.1 nm analyte on a dielectric layer (*e.g.*, a biorecognition interface) of a low thickness (lower than *ca.* 5 nm) is influenced primarily by the decay length, whereas the response for dielectric layers of higher thicknesses follows the RIS trend. In terms of transducer optimization, larger islands are advantageous for systems involving thick layers which occupy much of the sensing volume, hence the

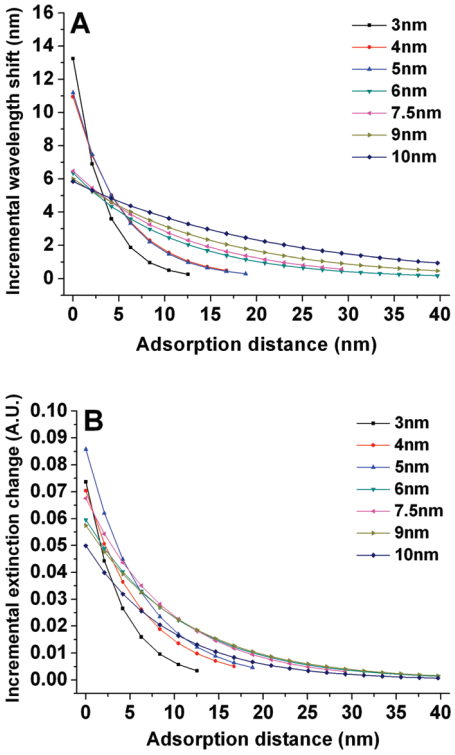

Figure 14. Calculated incremental wavelength shift (A) and extinction intensity change (B) for the adsoprtion of a 2.1-nm-thick polyelectrolyte bilayer on an existing polyelectrolyte multilayer of varying thickness; Au nominal thicknesses are indicated. Data points were obtained by substituting in eq 2 the experimental decay length and refractive index sensitivity values derived from the exponential regression (data from Figure 8).

large RIS values dominate; on the other hand, small islands exhibit higher sensitivities for thin layers, despite the lower RIS, owing to the better match of the decay length and sensing volume to the dielectric layer thickness. In the case of biological molecules, which are commonly a few nanometers in diameter, better optical response is expected with LSPR systems comprising smaller islands.

Therefore, plots such as those in Figure 14 can be used for rational design, namely, to predict the optimal transducer for detection of a binding event involving specific analyte and recognition layer of given dimensions.

As noted in the introduction, LSPR transducers display spatial inhomogeneity of the sensitivity, while our earlier work showing a linear response to analyte surface coverage indicated effective averaging of this effect in the present system. However, a possible correlation between spatially variable RIS and decay length may be studied in the future and used for further optimization.

The results shown in Figure 8 panels A and B require additional discussion. The values of the wavelength RIS m_λ increase with Au layer thickness (Figure 8A), while the corresponding intensity refractive index sensitivity m_{ext} reaches a maximum for 7.5 nm films, above which a decrease in the values is observed (Figure 8B).

To understand this apparent discrepancy it is useful to examine the physical basis of these variables. The two experimental parameters, m_λ and m_{ext}, are commonly treated in the same manner, as both are similarly used for sensing purposes. However, for a physical discussion the fundamental difference between the two becomes relevant. While the peak wavelength is a basic property of the islands which is independent of the quantity of particles in the optical path (other than coupling effects), the extinction intensity is an additive variable which depends directly on the amount of particles sampled. In the present case, a higher surface density of islands will not affect m_λ (neglecting plasmon coupling effects, which are minor here), but will lead to a higher extinction, and correspondingly, to a higher RIS m_{ext}. Therefore, while for sensing purposes the values of m_λ and m_{ext} are the relevant working parameters, for a discussion of physical aspects of the system, including a comparison of different island films, the value of m_{ext} should be normalized to the surface density of particles. The normalized parameter $\tilde{m}_{ext} = m_{ext}/c$, where c is the number of islands per unit surface area (see Table 1), is thus a quantity-independent variable, analogous to m_λ as an intrinsic physical property of the island ensemble.

Values of $\tilde{m}_{ext}$ *versus* film nominal thickness are plotted in Figure 8C. The normalized values display a generally monotonous increase with Au film thickness, similar to the behavior of m_λ (Figure 8A). Hence, while the larger islands display larger values of $\tilde{m}_{ext}$, their low surface density results in lower values of m_{ext}.

CONCLUSION

We have presented a systematic experimental study on the relationship between refractive index sensitivity (RIS) and plasmon decay length in Au-island-based localized plasmon transducers. The decay length was derived using polyelectrolyte LbL assembly and fitting to a model of exponentially decaying surface plasmon field. Since the polyelectrolyte multilayer covers both the Au islands and the glass substrate between the islands, experiments with site-selective adsorption as well as model calculations were carried out to assess the sensitivity to binding to the top *versus* the side faces of the islands, establishing the validity of our approach. The RIS was determined from the same exponential regression, as well as from measurements in solvents of different refractive index values. While the wavelength RIS, m_λ, shows a gradual increase with average island size, the extinction intensity RIS, m_{ext}, initially increases with average island size, reaching a maximum and decreasing upon further size increase. This seemingly contradicting behavior emphasizes the different physical nature of the two variables; that is, m_{ext} is dependent on the number of islands in the sampled area while m_λ is not. Hence, normalization of m_{ext} to the surface density of Au islands leads to a similar behavior to that of m_λ. It is concluded that the intensity RIS m_{ext} is a working parameter relevant to sensing applications; however, for a discussion of the physical significance of the RIS, a surface density normalized value $\tilde{m}_{ext}$ has to be calculated.

The results for a series of Au island films with varying average island size show a near-linear correlation between the RIS and decay length, the two parameters in eq 1 characteristic of a given transducer. This correlation undermines the assumption that in order to achieve higher LSPR transducer sensitivity the RIS has to be maximized. Instead, it is shown that optimization of LSPR transducers requires tailor-design; that is, a combination of RIS and decay length has to be chosen which maximizes the response to a specific analyte and recognition interface of given dimensions. In the case of biorecognition, where the typical molecular size is a few nanometers, small islands exhibiting lower RIS values are actually expected to provide a higher overall sensitivity, as a result of better matching of the decay length. Our conclusions regarding the interplay between RIS and decay length and its effect on system optimization are general and are expected to be relevant to other types of LSPR transducers as well.

METHODS

Materials. The substrates used were microscope glass coverslides (Schott AG borosilicate glass D263T No. 3, 22 × 22 mm^2, with $T_g \approx 557$ °C, supplied by Menzel-Gläser, Germany), cut to 22 × 9 mm^2; and quartz slides (Heraeus Quarzglas, Germany), 1 mm thick, cut to 37 × 12 mm^2. Gold (99.99%, Holland-Moran, Israel); polyallylamine hydrochloride (PAH) (56 kDa, Sigma Aldrich); polystyrene sulfonate, sodium salt (PSS) (70 kDa, Polysciences Inc., Warrington, PA, USA); 1-octadecanethiol (ODT) (98%, Aldrich); 2-[methoxy(polyethylenoxy)propyl]trimethoxysilane, 6−9 C_2H_4O groups (PEG-silane) (90%, Gelest); 3-aminopropyl trimethoxysilane (APTS) (Aldrich); sodium chloride (Frutarom, Israel); methanol (anhydrous, Mallinckrodt); ethanol (anhydrous, Gadot or Biolab, Israel); heptane (anhydrous, Aldrich); chloroform (Gadot); toluene (Gadot); H_2SO_4 (AR, Gadot); H_2O_2 (30%, Frutarom); and ammonium hydroxide (Frutarom), were used as received. Nitrogen was in-house supplied from liquid N_2. All solutions were prepared using triply distilled water.

Continuous Gold Films. The glass slides were cleaned in freshly prepared "piranha" solution (H_2O_2:H_2SO_4, 1:3 by volume) for 1 h, and washed with deionized water, then with triply distilled water, and finally with ethanol. (*Caution: "piranha" solution is extremely corrosive and boils upon mixing.*) The slides were then treated with an "RCA" solution ($H_2O/NH_4OH/H_2O_2$, 5:1:1 by volume) at approximately 70 °C for 1 h, to hydroxylate the surface, and modified with APTS by overnight immersion in 10% APTS (by volume) in methanol. APTS layers have been known to improve the adhesion of gold evaporated on glass substrates.[46] The slides were then washed in methanol, sonicated in methanol three times (5 min each), washed in ethanol, and dried under a nitrogen stream. A total of 24 slides were placed on a plate, which was mounted in a cryo-HV evaporator (Key High

Vacuum) equipped with a Maxtek TM-100 thickness monitor. The chamber was evacuated to a pressure of $2-3 \times 10^{-6}$ Torr, and gold was evaporated onto the slides from a resistively heated tungsten boat. The plate was rotated during evaporation to achieve homogeneous deposition on the slides. The 20 nm of gold was deposited at a rate of 0.1 nm/sec; at this thickness, the film is semitransparent and suitable for transmission spectroscopy.[46] The slides were then annealed at 200 °C for 20 h in a Ney Vulcan 3-550 furnace, at a 5 °C/min heating rate, then left to cool to room temperature inside the furnace. Gold films prepared using this procedure are smooth and can be studied by various surface techniques.[46]

Discontinuous (Island-Type) Gold Films. Glass slides were cleaned and mounted in the evaporation chamber as described above (without APTS coating). Gold was evaporated on the slides at a deposition rate of 0.01 nm/sec, to a nominal thicknesses of 3−10 nm (the nominal thickness is the reading of the evaporator QCM thickness monitor, *i.e.*, the film mass thickness). Following evaporation, the slides were annealed as detailed above for 10 h at 580 °C (5 °C/min heating rate), then left to cool to room temperature inside the furnace.

Polyelectrolyte LbL Assembly. The LbL procedure was carried out using the positive polyelectrolyte poly(allylamine hydrochloride) (PAH) and the negative polyelectrolyte poly(styrene sulfonate), sodium salt (PSS), 1.0 mM solutions (concentration calculated with respect to the monomer, corresponding to 0.093 mg mL^{-1} PAH and 0.206 mg mL^{-1} PSS) in 0.1 M NaCl in triply distilled water. Au films prepared as detailed above were treated 10 min in a UV/ozone apparatus (UVOCS Inc., model T10*10/OES/E), with the Au coating facing the UV lamps. The samples were then washed 20 min in ethanol[47] and dried under a nitrogen stream. The slide to be coated was alternatingly immersed in vials containing the polyelectrolyte solutions for 15 min each, starting with PAH. After each adsorption step the slide was rinsed with water, dipped into an aqueous solution of 0.1 M NaCl, and immersed in the other polyelectrolyte solution. After completing the assembly of a number of polyelectrolyte bilayers the slide was washed and dried under a nitrogen stream, measured, and the LbL procedure was resumed. The adsorption and measurements were carried out in a climate-controlled laboratory, at a temperature of 22.5 ± 1.0 °C and a humidity of $50 \pm 5\%$.

Site-Selective Adsorption. Au island slides were treated in the UV/ozone apparatus and washed in ethanol as detailed above. ODT was adsorbed by immersing the slide in a 1 mM ODT ethanolic solution for 1 h. PEG−silane was adsorbed similarly from a freshly prepared 2 mM PEG−silane ethanolic solution, for 2 h. Adsorption of both SAMs was followed by a 20 min wash in ethanol and drying. For each Au thickness studied, four slides were coated with ODT followed by PEG−silane, and four were coated with PEG−silane followed by ODT.

Characterization. Extinction spectra at normal incidence of polyelectrolyte multilayers were measured using a Varian Carey 50 probe UV/vis spectrophotometer. Measurement parameters were as follows: wavelength resolution, 1 nm; scan rate, 300 nm/min; average acquisition time per point, 0.2 s. For dry measurements, air was used as the baseline; for measurements in a given solvent, a cuvette filled with the same solvent, without a slide, was used as baseline. Spectra of SAMs (ODT, PEG-silane) were measured at 0.2 nm resolution using the Varian Carey spectrophotometer or an Ocean Optics USB4000XR spectrophotometer equipped with a Polychromix MobiLight light source. Polyelectrolyte film thickness on continuous gold slides was measured in air using an Angstrom Advanced PhE-102 spectroscopic ellipsometer, at an angle of incidence of 70°, in the spectral range 300−800 nm, using 1−20 nm steps. The high-resolution measurements were used to develop a model, which was then used for analyzing the lower-resolution measurements. Ellipsometric data were analyzed using Film Wizard software (Scientific Computing International, California, USA). High-resolution scanning electron microscopy (HRSEM) images were obtained using a Carl Zeiss Ultra-55 ultrahigh-resolution SEM. The samples were coated with a thin layer of Cr (2 nm Cr on 3−5 nm Au, 3 nm Cr on 6−10 nm Au), for improved conductivity.

Image Analysis. HRSEM images of Au island films of various nominal thickness were analyzed using ImageJ image analysis software (Wayne Rasband, NIH, USA), to determine particle dimensions and size distribution. The average distance between islands was calculated as the average distance between the particle centers, to the four nearest neighbors. In addition, the surface density of islands for the various Au film thicknesses was calculated; half of the particles crossing edges were counted. These calculations were based on the same HRSEM images used for particle size analysis.

Acknowledgment. Support of this work by the Israel Science Foundation, Grant No. 672/07, and by the Minerva Foundation with funding from the Federal German Ministry for Education and Research, is gratefully acknowledged. The electron microscopy studies were conducted at the Irving and Cherna Moskowitz Center for Nano and Bio-Nano Imaging, Weizmann Institute of Science. This research is made possible in part by the historic generosity of the Harold Perlman family.

Supporting Information Available: UV−vis spectra of polyelectrolyte multilayers on Au island films; ellipsometric thickness of polyelectrolyte films; differential wavelength and extinction intensity response to adsorption; site-selective adsorption calculations. This material is available free of charge *via* the Internet at http://pubs.acs.org.

REFERENCES AND NOTES

1. Haes, A. J.; Van Duyne, R. P. A Unified View of Propagating and Localized Surface Plasmon Resonance Biosensors. *Anal. Bioanal. Chem.* **2004,** *379*, 920–930.
2. Stewart, M. E.; Anderton, C. R.; Thompson, L. B.; Maria, J.; Gray, S. K.; Rogers, J. A.; Nuzzo, R. G. Nanostructured Plasmonic Sensors. *Chem. Rev.* **2008,** *108*, 494–521.
3. Evanoff, D. D. J.; Chumanov, G. Synthesis and Optical Properties of Silver Nanoparticles and Arrays. *ChemPhysChem* **2005,** *6*, 1221–1231.
4. Link, S.; El-Sayed, M. A. Spectral Properties and Relaxation Dynamics of Surface Plasmon Electronic Oscillations in Gold and Silver Nanodots and Nanorods. *J. Phys. Chem. B* **1999,** *103*, 8410–8426.
5. McFarland, A. D.; Van Duyne, R. P. Single Silver Nanoparticles as Real-Time Optical Sensors with Zeptomole Sensitivity. *Nano Lett.* **2003,** *3*, 1057–1062.
6. Vaskevich, A.; Rubinstein, I., Localized Surface Plasmon Resonance (LSPR) Spectroscopy in Biosensing. In *Handbook of Biosensors and Biochips*; Marks, R., Cullen, D., Lowe, C., Weetall, H. H., Karube, I., Eds.; Wiley: Chichester, UK, 2007.
7. Karakouz, T.; Holder, D.; Goomanovsky, M.; Vaskevich, A.; Rubinstein, I. Morphology and Refractive Index Sensitivity of Gold Island Films. *Chem. Mater.* **2009,** *21*, 5875–5885.
8. Malinsky, M. D.; Kelly, K. L.; Schatz, G. C.; Van Duyne, R. P. Chain Length Dependence and Sensing Capabilities of the Localized Surface Plasmon Resonance of Silver Nanoparticles Chemically Modified with Alkanethiol Self-Assembled Monolayers. *J. Am. Chem. Soc.* **2001,** *123*, 1471–1482.
9. Jung, L. S.; Campbell, C. T.; Chinowsky, T. M.; Mar, M. N.; Yee, S. S. Quantitative Interpretation of the Response of Surface Plasmon Resonance Sensors to Adsorbed Films. *Langmuir* **1998,** *14*, 5636–5648.
10. Haes, A. J.; Van Duyne, R. P. A Nanoscale Optical Biosensor: Sensitivity and Selectivity of an Approach Based on the Localized Surface Plasmon Resonance Spectroscopy of Triangular Silver Nanoparticles. *J. Am. Chem. Soc.* **2002,** *124*, 10596–10604.
11. Bendikov, T. A.; Rabinkov, A.; Karakouz, T.; Vaskevich, A.; Rubinstein, I. Biological Sensing and Interface Design in Gold Island Film Based Localized Plasmon Transducers. *Anal. Chem.* **2008,** *80*, 7487–7498.
12. Svedendahl, M.; Chen, S.; Dmitriev, A.; Käll, M. Refractometric Sensing Using Propagating *versus* Localized Surface Plasmons: A Direct Comparison. *Nano Lett.* **2009,** *9*, 4428–4433.
13. Nath, N.; Chilkoti, A. Label-free Biosensing by Surface Plasmon Resonance of Nanoparticles on Glass: Optimization of Nanoparticle Size. *Anal. Chem.* **2004,** *76*, 5370–5378.

14. Nusz, G. J.; Curry, A. C.; Marinakos, S. M.; Wax, A.; Chilkoti, A. Rational Selection of Gold Nanorod Geometry for Label-free Plasmonic Biosensors. *ACS Nano* **2009,** *3*, 795–806.
15. Haynes, C. L.; Van Duyne, R. P. Nanosphere Lithography: A Versatile Nanofabrication Tool for Studies of Size-Dependent Nanoparticle Optics. *J. Phys. Chem. B* **2001,** *105*, 5599–5611.
16. Haes, A. J.; Zou, S.; Schatz, G. C.; Van Duyne, R. P. Nanoscale Optical Biosensor: Short Range Distance Dependence of the Localized Surface Plasmon Resonance of Noble Metal Nanoparticles. *J. Phys. Chem. B* **2004,** *108*, 6961–6968.
17. Haes, A. J.; Zou, S.; Schatz, G. C.; Van Duyne, R. P. A Nanoscale Optical Biosensor: The Long Range Distance Dependence of the Localized Surface Plasmon Resonance of Noble Metal Nanoparticles. *J. Phys. Chem. B* **2004,** *108*, 109–116.
18. Whitney, A. V.; Elam, J. W.; Zou, S.; Zinovev, A. V.; Stair, P. C.; Schatz, G. C.; Van Duyne, R. P. Localized Surface Plasmon Resonance Nanosensor: A High-Resolution Distance-Dependence Study Using Atomic Layer Deposition. *J. Phys. Chem. B* **2005,** *109*, 20522–20528.
19. Okamoto, T.; Yamaguchi, I.; Kobayashi, T. Local Plasmon Sensor with Gold Colloid Monolayers Deposited Upon Glass Substrates. *Opt. Lett.* **2000,** *25*, 372–374.
20. Doron-Mor, I.; Cohen, H.; Barkay, Z.; Shanzer, A.; Vaskevich, A.; Rubinstein, I. Sensitivity of Transmission Surface Plasmon Resonance (T-SPR) Spectroscopy: Self-Assembled Multilayers on Evaporated Gold Island Films. *Chem.—Eur. J.* **2005,** *11*, 5555–5562.
21. Rindzevicius, T.; Alaverdyan, Y.; Käll, M.; Murray, W. A.; Barnes, W. L. Long-Range Refractive Index Sensing Using Plasmonic Nanostructures. *J. Phys. Chem. C* **2007,** *111*, 11806–11810.
22. Murray, W. A.; Suckling, J. R.; Barnes, W. L. Overlayers on Silver Nanotriangles: Field Confinement and Spectral Position of Localized Surface Plasmon Resonances. *Nano Lett.* **2006,** *6*, 1772–1777.
23. Szunerits, S.; Das, M. R.; Boukherroub, R. Short- and Long-Range Sensing on Gold Nanostructures, Deposited on Glass, Coated with Silicon Oxide Films of Different Thicknesses. *J. Phys. Chem. C* **2008,** *112*, 8239–8243.
24. Haes, A. J.; Zou, S.; Schatz, G. C.; Van Duyne, R. P.; Nanoscale, A Optical Biosensor: The Long Range Distance Dependence of the Localized Surface Plasmon Resonance of Noble Metal Nanoparticles. *J. Phys. Chem. B* **2004,** *108*, 109–116.
25. Marie, R.; Dahlin, A. B.; Tegenfeldt, J. O.; Höök, F. Generic Surface Modification Strategy for Sensing Applications Based on Au/SiO_2 Nanostructures. *Biointerphases* **2007,** *2*, 49–55.
26. Kalyuzhny, G.; Schneeweiss, M. A.; Shanzer, A.; Vaskevich, A.; Rubinstein, I. Differential Plasmon Spectroscopy as a Tool for Monitoring Molecular Binding to Ultrathin Gold Films. *J. Am. Chem. Soc.* **2001,** *123*, 3177–3178.
27. Kalyuzhny, G.; Vaskevich, A.; Ashkenasy, G.; Shanzer, A.; Rubinstein, I. UV/Visible Spectroscopy of Metalloporphyrin and Metallophthalocyanine Monolayers Self-Assembled on Ultrathin Gold Films. *J. Phys. Chem. B* **2000,** *104*, 8238–8244.
28. Decher, G.; Hong, J.; Schmitt, J. Buildup of Ultrathin Multilayer Films by a Self-Assembly Process: III. Consecutively Alternating Adsorption of Anionic and Cationic Polyelectrolytes on Charged Surfaces. *Thin Solid Films* **1992,** *210—211*, 831–835.
29. Klitzing, V. R.; Wong, J. E.; Jargerc, W.; Steitz, R. Short Range Interactions in Polyelectrolyte Multilayers. *Curr. Opin. Colloid Interface Sci.* **2004,** *9*, 158–162.
30. Decher, G. Fuzzy Nanoassemblies: Toward Layered Polymeric Multicomposites. *Science* **1997,** *277*, 1232–1237.
31. Büscher, K.; Graf, K.; Ahrens, H.; Helm, C. A. Influence of Adsorption Conditions on the Structure of Polyelectrolyte Multilayers. *Langmuir* **2002,** *18*, 3585–3591.
32. Bertrand, P.; Jonas, A.; Laschewsky, A.; Legras, R. Ultrathin Polymer Coatings by Complexation of Polyelectrolytes at Interfaces: Suitable Materials, Structure and Properties. *Macromol. Rapid Commun.* **2000,** *21*, 319–348.
33. Karakouz, T.; Tesler, A. B.; Bendikov, T. A.; Vaskevich, A.; Rubinstein, I. Highly Stable Localized Plasmon Transducers Obtained by Thermal Embedding of Gold Island Films on Glass. *Adv. Mater.* **2008,** *20*, 3893–3899.
34. Tesler, A. B.; Chuntonov, L.; Karakouz, T.; Bendikov, T. A.; Haran, G.; Vaskevich, A.; Rubinstein, I. In preparation.
35. Hoda, N.; Larson, R. G. Modeling the Buildup of Exponentially Growing Polyelectrolyte Multilayer Films. *J. Phys. Chem. B* **2009,** *113*, 4232–4241.
36. Schneider, G.; Decher, G. From Functional Core/Shell Nanoparticles Prepared *via* Layer-by-Layer Deposition to Empty Nanospheres. *Nano Lett.* **2004,** *4*, 1833–1839.
37. Han, J.; Wang, X.; Kwok, D. Y., Structure and Stability of Self-Assembled Monolayers for Octadecanethiol Adsorbed on Flame Annealing Gold Substrate and Its Potential Application to Microfluidics. Proceedings of the 2004 International Conference on MEMS, NANO and Smart Systems, 2004. ICMENS 2004; 2004, Vol. *3*, pp 20-23.
38. Papra, A.; Gadegaard, N.; Larsen, N. B. Characterization of Ultrathin Poly(ethylene glycol) Monolayers on Silicon Substrates. *Langmuir* **2001,** *17*, 1457–1460.
39. Tesler, A. B.; Bendikov, T. A.; Vaskevich, A.; Rubinstein, I. In preparation.
40. Nath, N.; Chilkoti, A. Label-Free Colorimetric Biosensing Using Nanoparticles. *J. Fluorescence* **2004,** *14*, 377–389.
41. Kedem, O.; Vaskevich, A.; Rubinstein, I. In preparation.
42. Miller, M. M.; Lazarides, A. A. Sensitivity of Metal Nanoparticle Surface Plasmon Resonance to the Dielectric Environment. *J. Phys. Chem. B* **2005,** *109*, 21556–21565.
43. Liz-Marzán, L. M.; Giersig, M.; Mulvaney, P. Synthesis of Nanosized Gold—Silica Core—Shell Particles. *Langmuir* **1996,** *12*, 4329–4335.
44. Schmitt, J.; Mächtle, P.; Eck, D.; Möhwald, H.; Helm, C. A. Preparation and Optical Properties of Colloidal Gold Monolayers. *Langmuir* **1999,** *15*, 3256–3266.
45. Sannomiya, T.; Sahoo, P. K.; Mahcicek, D. I.; Solak, H. H.; Hafner, C.; Grieshaber, D.; Vörös, J. Biosensing by Densely Packed and Optically Coupled Plasmonic Particle Arrays. *Small* **2009,** *5*, 1889–1896.
46. Wanunu, M.; Vaskevich, A.; Rubinstein, I. Widely-Applicable Gold Substrate for the Study of Ultrathin Overlayers. *J. Am. Chem. Soc.* **2004,** *126*, 5569–5576.
47. Ron, H.; Matlis, S.; Rubinstein, I. Self-Assembled Monolayers on Oxidized Metals. 2. Gold Surface Oxidative Pretreatment, Monolayer Properties, and Depression Formation. *Langmuir* **1998,** *14*, 1116–1121.